4. Results and Discussion

To familiarize the reader with the history which motivated the current effort one must go back a year and a half, when Dr. Mahan met with Larry Langley, the owner Vatell Corporation. Vatell develops, manufactures and sells thermopile heat flux micro-sensors based on new patented technologies. The performance characteristics of these sensors, including the sensitivity, the time response and the dimensions were very promising. In February, 1996, the Thermal Radiation Group (TRG) of Virginia Tech entered into an agreement with Vatell, in which the TRG would provide a dynamic thermal model of the original thermopile design. At that time a parametric study was performed to optimize the sensitivity of the device. All the results from this original thermopile design can be found in a report submitted for the "Diplôme d'études approfondies (DEA)" to the Institut Universitaire des Systèmes Thermiques Industriels in June, 1996 [Weckmann, 1996]. In August, 1996, Dr. Mahan proposed to NASA a new variation on the Vatell sensor in a competition for the detector to be used on the GERB instrument. This proposal was accepted and the current efforts are aimed at providing the GERB instrument with a highly sensitive and reliable sensor.

To summarize in a few words, the goals are to predict the sensitivity and the time response characteristics of the latest sensor design and to optimize this design by using the dynamic electrothermal model in a parametric study. All of the results presented in this chapter are analytical and so have to be used with full knowledge of their limitations. They are offered here in support of the experimental results in a way that permits the manufacturing process to be optimized.

This chapter is organized into three parts. In the first part results of the one-dimensional and

two-dimensional models, including the sensitivity and the time response, are presented and are compared to the experimental results obtained by Vatell Corporation. In the second part, by exercising different model boundary conditions and changing critical parts of the geometry, a first attempt at design optimization is made. Finally, in the third part we investigate the basic assumption inherent to the model that no current flows in the device. This last part raises many questions, unanswered for the most part, but nevertheless interesting from the physical point of view.

4.1 One-Dimensional and Two-Dimensional Model Results

4.1.1 Temperature distribution

The steady-state temperature distributions calculated with the thermocouple one-dimensional and two-dimensional models are displayed in Figures 4.1 and 4.2, respectively. The one-dimensional model represents an ideal thermocouple in which the active junction is modeled as infinite in lateral dimensions. This is the ideal configuration for the thermocouple design because no heat is transfered in a second dimension and so the sensitivity is maximized. Following theory, the isotherms are perpendicular to the different layers of material in this model while the temperature distribution reflects the symmetry of the geometry and the boundary conditions. The heat is conducted only in the vertical plane. Most of the temperature gradient occurs in the thermal impedance layer of parylene, as expected.

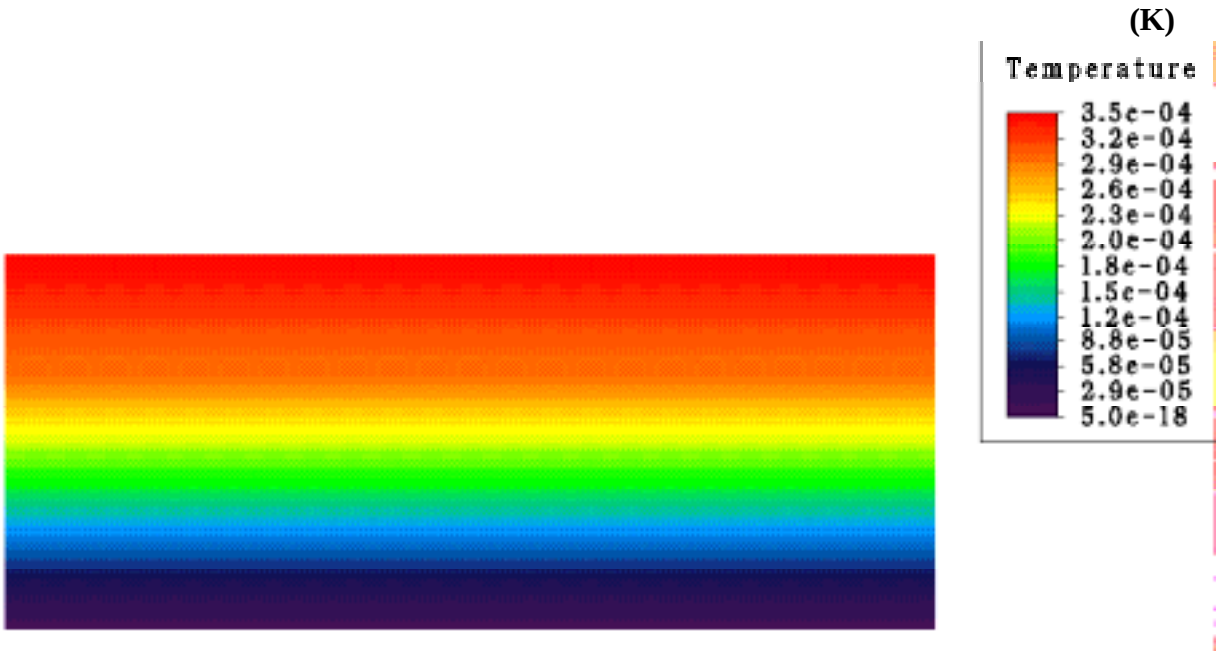

Figure 4.1. The steady-state one-dimensional temperature distribution for the boundary conditions shown in Figure 3.6.

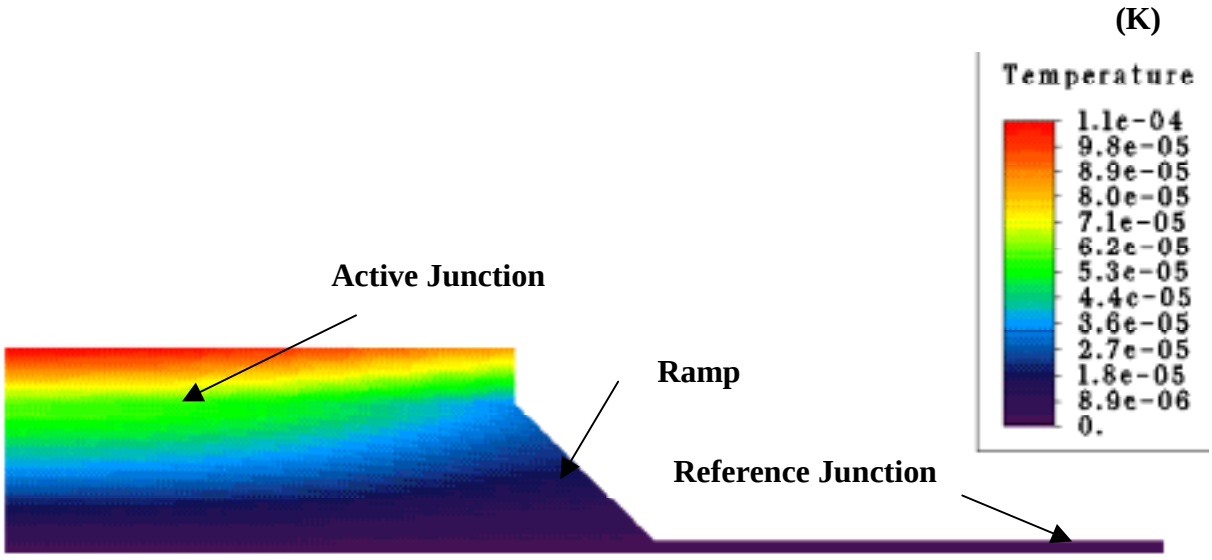

Figure 4.2. The steady-state two-dimensional temperature distribution corresponding to the boundary conditions of Figure 3.9

In the two-dimensional model, the isotherms are no longer perpendicular to the different layers of material in the region near the ramp connecting the active junction and the reference junction. The ramp permits divergence of the temperature field from the vertical; the heat flux is partially conducted in the horizontal plane as a result of the ramp. This effect and the fact that the heat sink is twice as big as the heat source (active junction) allow a smaller average temperature difference between the active junction and the reference junction than in the case of the one-dimensional model. For this reason it is predicted that the two-dimensionality of the thermocouple will decrease its sensitivity. The following provides more details about the sensitivity.

4.1.2 Sensitivity

A numerical sensitivity study has been conducted so as to quantify the ability of the thermocouple to sense a unit amount of radiant energy arriving at the active junction. Used were a nominal value of the Seebeck coefficient for the zinc-antimonide couple $S_{ZnSb-Pt}$, equal to 920 μV/K, and a heat flux input q´´ equal to 1 W/m^2. The sensitivity (V/Wm^{-2}) can be expressed as

$$\text{Sensitivity} = \frac{S_{ZnSb-Pt}\ \Delta T}{q''} \quad , \tag{4.1}$$

where ΔT (K) is the temperature difference between the active and reference junctions.

According to the literature [Pollock, 1985] the sensitivity of a thermocouple device can be evaluated by measuring the difference in temperature between the active, or “hot,” junction and the reference, or “cold,” junction. In the current case the thermocouple device is slightly different from the usual design of thermocouples due to the extremely small size of its junctions. The ratio, r, of the combined length of the junction to the length of the connecting leads has a value of five in the current design, whereas usually thermocouples have a ratio close to zero. This difference is illustrated in Figure 4.3.

The problem is to decide what temperature to assign to a junction in the case where the temperature is not uniform along the length of the junction, as is the case for the two-dimensional model. Figure 4.4 shows the temperature profile along the active junction. An overall temperature difference of 1.213×10^{-5} K is predicted between the two ends of a 60-μm active junction, compared

to a mean temperature difference between the active and reference junctions of 2.228×10^{-5} K. The mean junction temperature is obtained by averaging the temperature along the nodes lying within the plane of the junctions. Thus the temperature gradient represents 54 percent of the mean temperature.

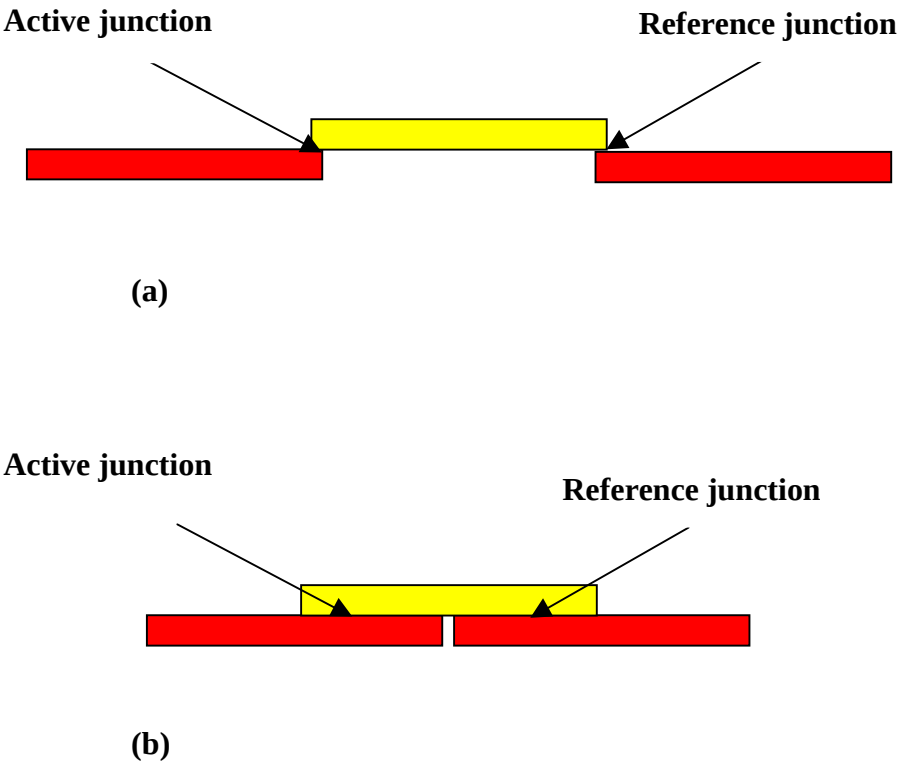

Figure 4.3. Comparison between different type of junctions: (a) the typical design and (b) the current design.

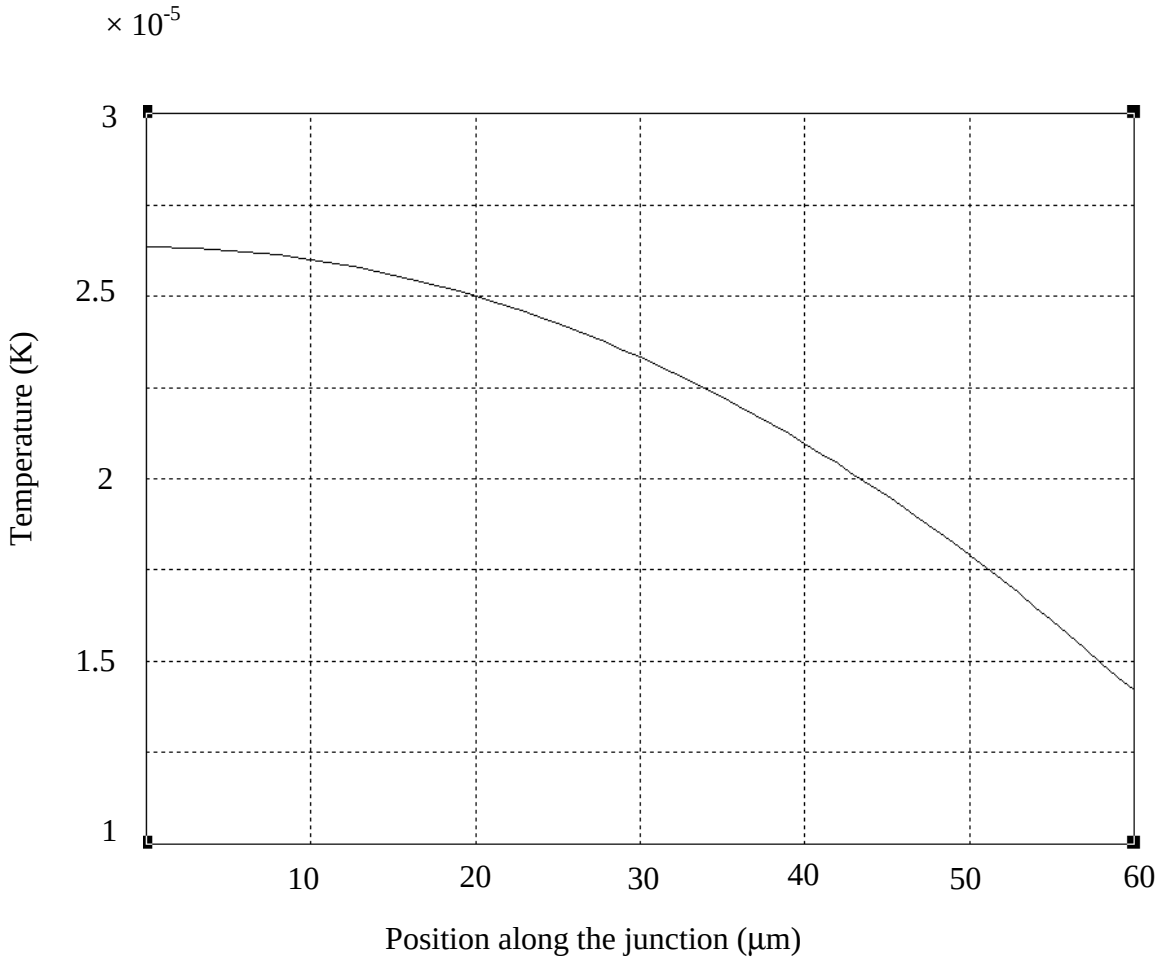

Figure 4.4. Temperature profile along the active junction

As for the reference junction, its temperature is essentially uniform; the temperature difference between its ends is smaller than 1.0×10^{-8} K and remains near the temperature of the heat sink (0 K)[1]. Thus, we will assume that the entire reference junction is kept at a uniform fixed temperature of 0 K. As a result only the temperature of the active junction influences the sensitivity of the instrument.

Since no accepted methods could be found in the literature for treating a thermocouple junction with an internal temperature gradient, it was decided to calculate the sensitivity two different ways. The first way is to take the highest local junction temperature as being representative of the temperature of the entire junction. This assumption is based on the law of successive temperatures, which states that a junction can be modeled as a series of small junctions with intermediate temperatures. The hot junction temperature is the highest temperature of the junction and the cold junction temperature is the lowest, as illustrated in Figure 4.5.

[1] The calculations are made on the basis of a relative temperature of T-311 K, as described in Section 3.3.2

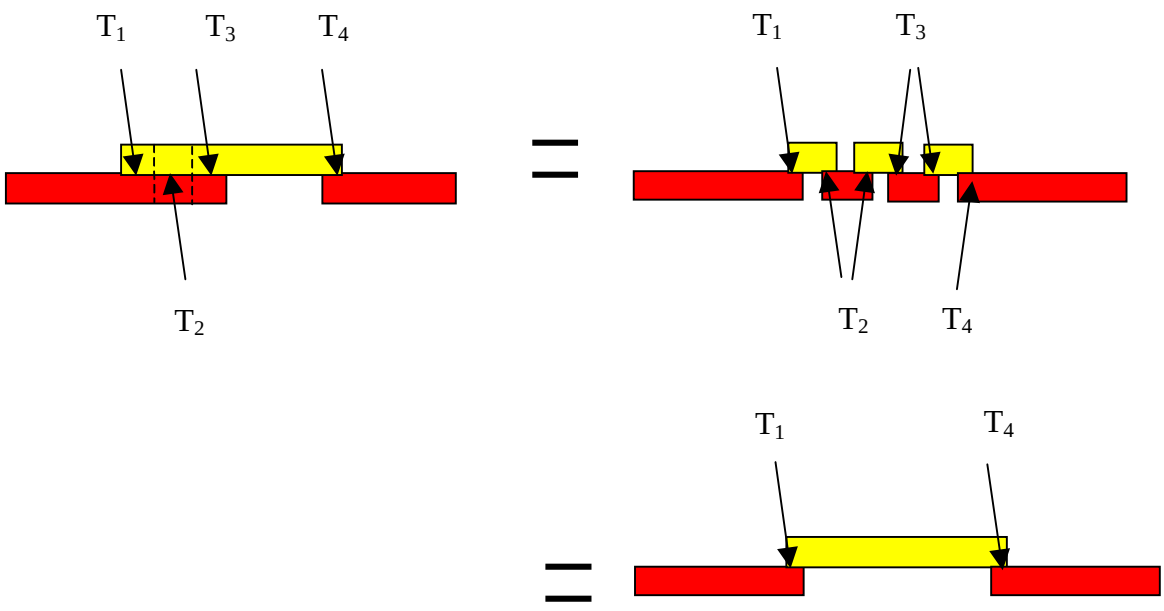

Figure 4.5. The law of intermediate temperatures applied to our model.

The second way that sensitivity is calculated is to take the average temperature at the junction. This assumption is based on the fact that we do not really know where to locate the effective junction in our model. This question has not been answered in the literature found on solid-state physics, but it must somehow be taken into consideration. To partially solve the problem of where to locate the effective junction, the sensitivity has been calculated for different candidate junction locations. The so-called “upper junction”, “physical junction” and “lower junction” are shown in Figure 4.6.

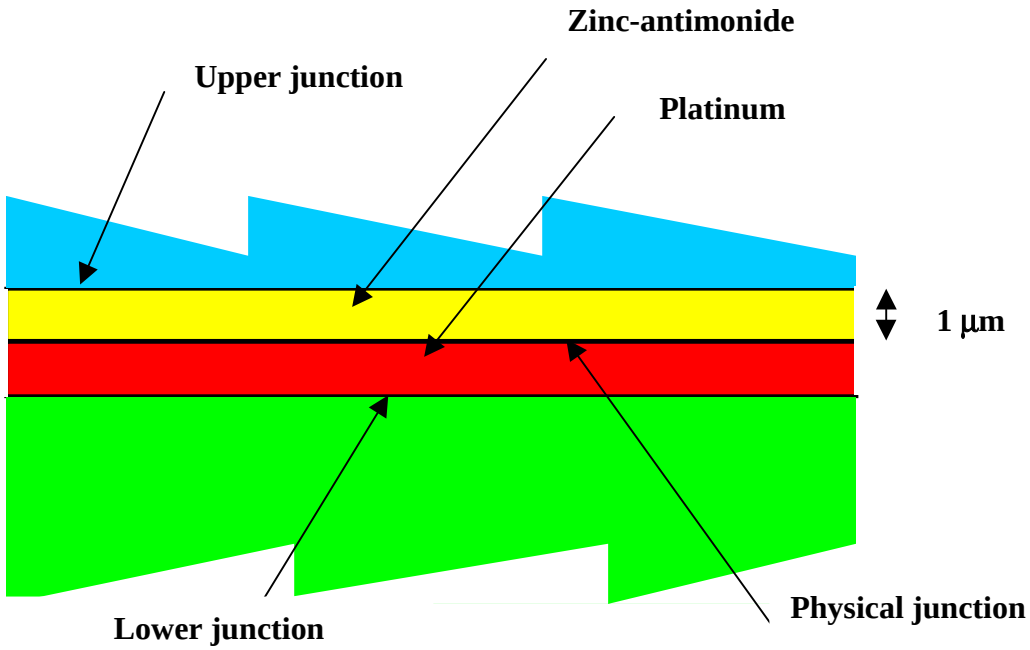

Figure 4.6. Definition of three different candidate junctions according to their locations

Table 4.1 shows the sensitivity obtained by averaging the temperature along the nodes lying within the planes of the three different junction definitions.

Table 4.1. Effect of junction definition on the predicted sensitivity

	Upper Junction	**Physical Junction**	**Lower Junction**
Sensitivity ($\mu V/Wm^{-2}$)	0.04626	0.04624	0.04623

Since no significant difference (less than 0.03 percent) in the predicted sensitivity for the three different junctions was found, the average temperature at the physical junction is used in this thesis.

To study sensitivity, two different two-dimensional configurations have been modeled. The first configuration involves an active junction of 60-μm length, and the second involves an active junction of 93-μm length. The length of the reference junction remains at 93 μm for both configurations. The length of the connecting ramp (25.4 μm) remains the same in both configurations. These two configurations are used to study the two-dimensionality of the problem. The effect of the two-dimensionality is greater in the first configuration because the aspect ratio between the active junction and the ramp connecting it to the reference junction is smaller compared to the second configuration (0.33 for the first configuration and 0.44 for the second configuration). The predicted sensitivities of the one-dimensional and two-dimensional models are presented in Table 4.2

Table 4.2. Sensitivity of the detector based on the one-dimensional and two-dimensional models.

	Sensitivity[1] ($\mu V/W.m^{-2}$) based on the average temperature	Sensitivity[2] ($\mu V/W.m^{-2}$) based on the highest temperature	Improvement of column 2 results over those of column 3 (percent)
One-dimensional model	0.278	0.278	0
Two-dimensional model (first configuration:60-μm length)	0.0205	0.0242	15.3
Two-dimensional model (second configuration 93-μm length)	0.0462	0.0543	14.9

[1] Sensitivity calculated based on the average junction temperature
[2] Sensitivity calculated based upon the highest local temperature at the junction

As anticipated, the sensitivity decreases as the two-dimensionality of the model increases. In other words the sensitivity decreases as the size of the ramp becomes bigger compared to the length of the active junction. These results show a significant difference in sensitivity depending upon how the junction temperature is defined. If the temperature at the junction is assumed to be the highest temperature, the value of the sensitivity is increased by more than 15 percent. This difference increases with the two-dimensionality (or inverse of the aspect ratio) of the model.

4.1.3 The time response

The concept of detector time constant is based upon the premise that the detector responds as a first-order system to a step input applied at time t = 0. This assumption is justified if the detector is modeled with heat capacitance C (J/K) and a thermal conductance K (W/K) between the detector and the heat sink. More details on this simple thermal model are given in Section 2.2.3.

If the detector responds as a first-order system, its temperature response as a function of time for a step input at time t = 0 can be modeled as

$$T'(t) = T_{final}\,[1 - e^{-t/\tau}], \tag{4.2}$$

where τ is the time constant and T_{final} is the steady-state temperature. The time constant of the first-order system is defined as the time necessary for the response to reach 63.2 percent of its steady-state value.

The temperature response of the junction has been computed with the dynamic model developed using the finite element tool ALGOR. In order to compare the analytical results with the model of Equation 4.2 we used a least-squares best-fit analysis. With the least-squares method the time constant τ is selected to minimize the sum of the squared deviations of the finite element data points from the theory of Equation 4.2. In other words, we minimize the quantity

$$\sum_{i=1}^{nstep} [T_i - T_i']^2 \quad , \tag{4.3}$$

where T_i and T'_i are the calculated finite element and modeled (Equation 4.2) temperatures, respectively, at the i^{th} time step t_i.

This implies that

$$\frac{\partial}{\partial \tau}\left\{\sum_{i=1}^{nstep}[T_i - T_i']^2\right\} = 0 \quad . \tag{4.4}$$

Differentiating yields

$$\sum_{i=1}^{nstep} \frac{t_i}{\tau} \exp(-t_i/\tau)[T_i - T_i']^2 \quad = \quad 0 \quad . \tag{4.5}$$

Solving Equation 4.5 gives the value of the time constant τ in the least-squares sense.

To determine how accurately the temperatures calculated with the finite element model match the temperatures calculated with the first order model, the root-mean-square (rms) error,

$$\text{rms} = \frac{1}{\text{nstep}} \sqrt{\sum_{i=1}^{nstep}[T_i - T_i']^2} \quad , \tag{4.6}$$

was computed, where nstep is the number of steps.

Before running any transient cases on ALGOR a study to optimize the value of the time step increment had to be carried out for both the one-dimensional and two-dimensional models. Plotting the highest model junction node temperature attained for different time steps has provided a value of time step which gives converged results. These plots can be found in Figures 4.7 and 4.8 for the one-dimensional model and the two-dimensional model (second configuration), respectively. An optimized time step of 1.0×10^{-4} s has been chosen for the one-dimensional model, and a 1.0×10^{-5} s time step for the two-dimensional model.

In order to calculate the time constant of the device, a study must be conducted to assess the influence of the assumed effective junction node location on the time response. The time constant may be sensitive to the assumed location of the junction in the two-dimensional model, since some of the thermal energy diverges through the ramp from the active junction towards the reference junction. This effect may modify the time constant of the device depending on which node is used to define the active junction temperature. For this study the time constant has been calculated for different node locations in the active junction, for each of two different model geometrical configurations. The first configuration has a shorter active junction than the second configuration

so as to assess the effect of the two-dimensionality. The effect of the two-dimensionality is bigger in the first configuration where the active junction is smaller (i.e the aspect ratio is smaller).

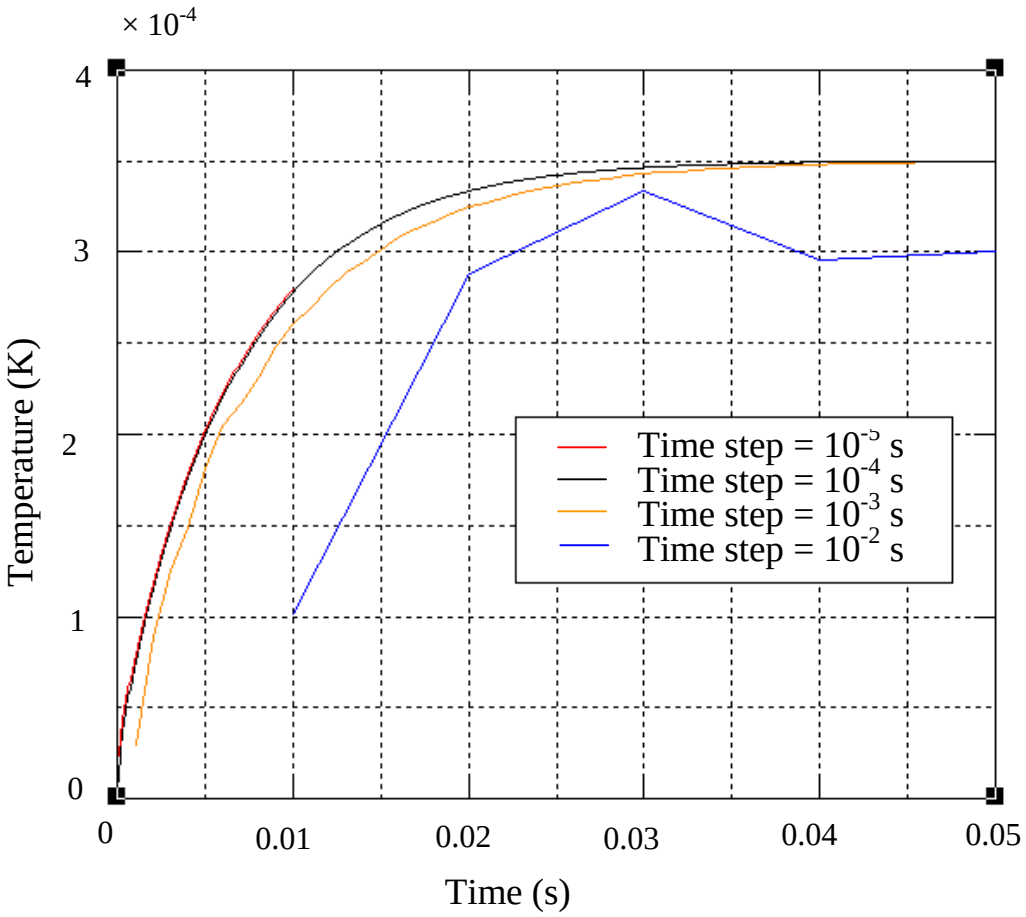

Figure 4.7. One-dimensional model time step optimization

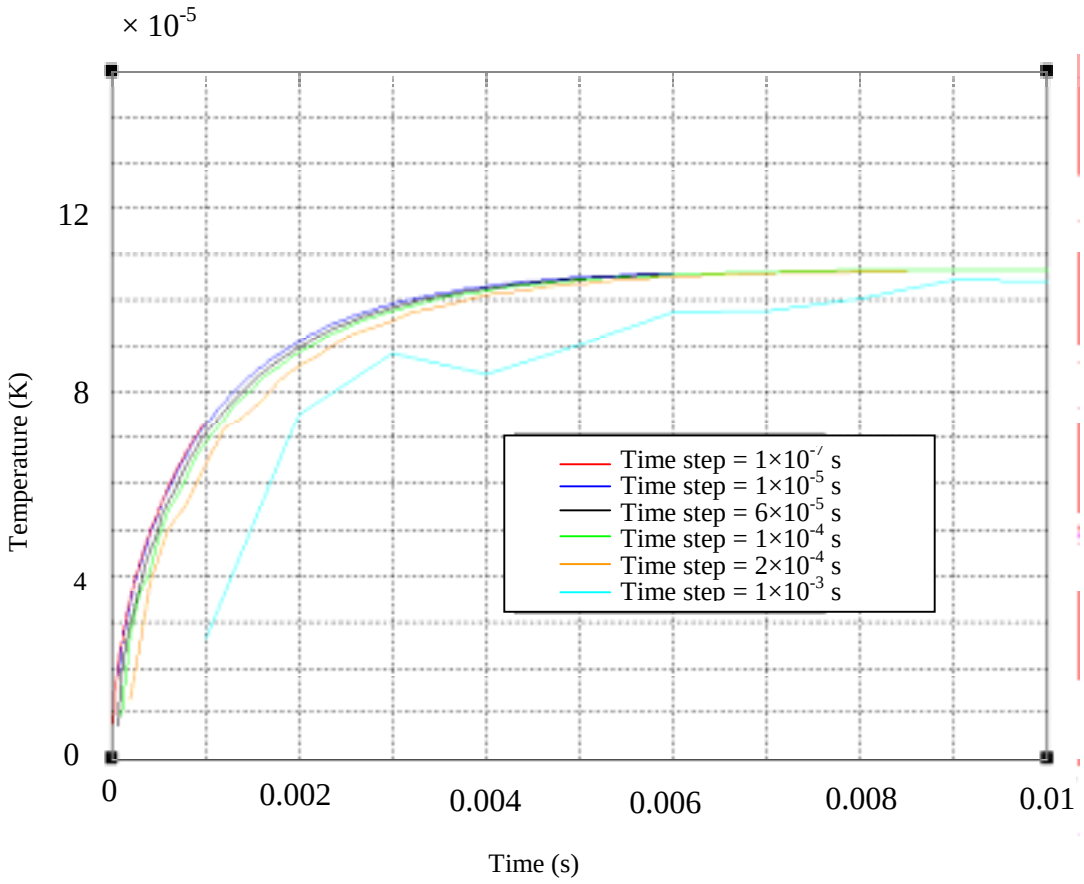

Figure 4.8. Two-dimensional model time step optimization

Nodes at five different locations in the plane of the junction of the thermocouple were selected for the first geometrical configuration (i.e having an active junction length of 60 μm). They have been regularly selected with a 15-μm space separating them. These node locations may be seen in Figure 4.9. The time response corresponding to the different nodes is depicted in Figure 4.10.

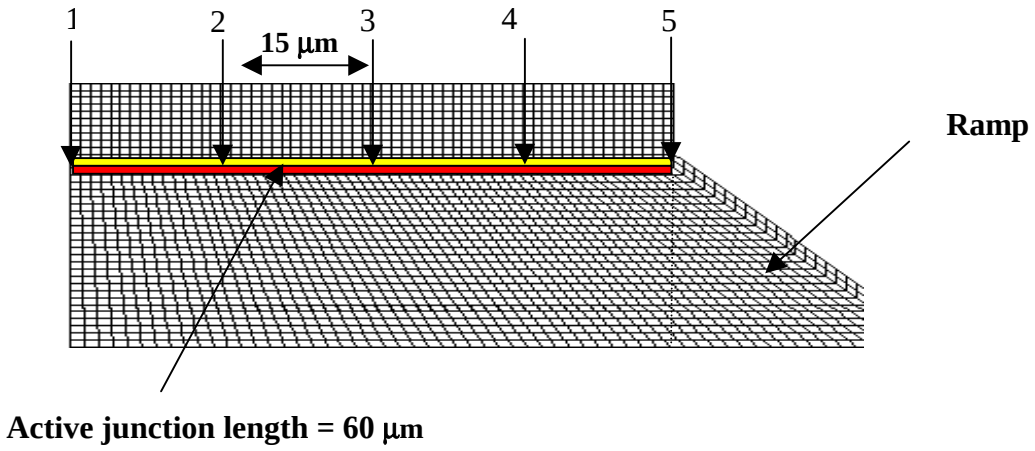

Figure 4.9. Junction nodes selected (active junction length of 60 μm)

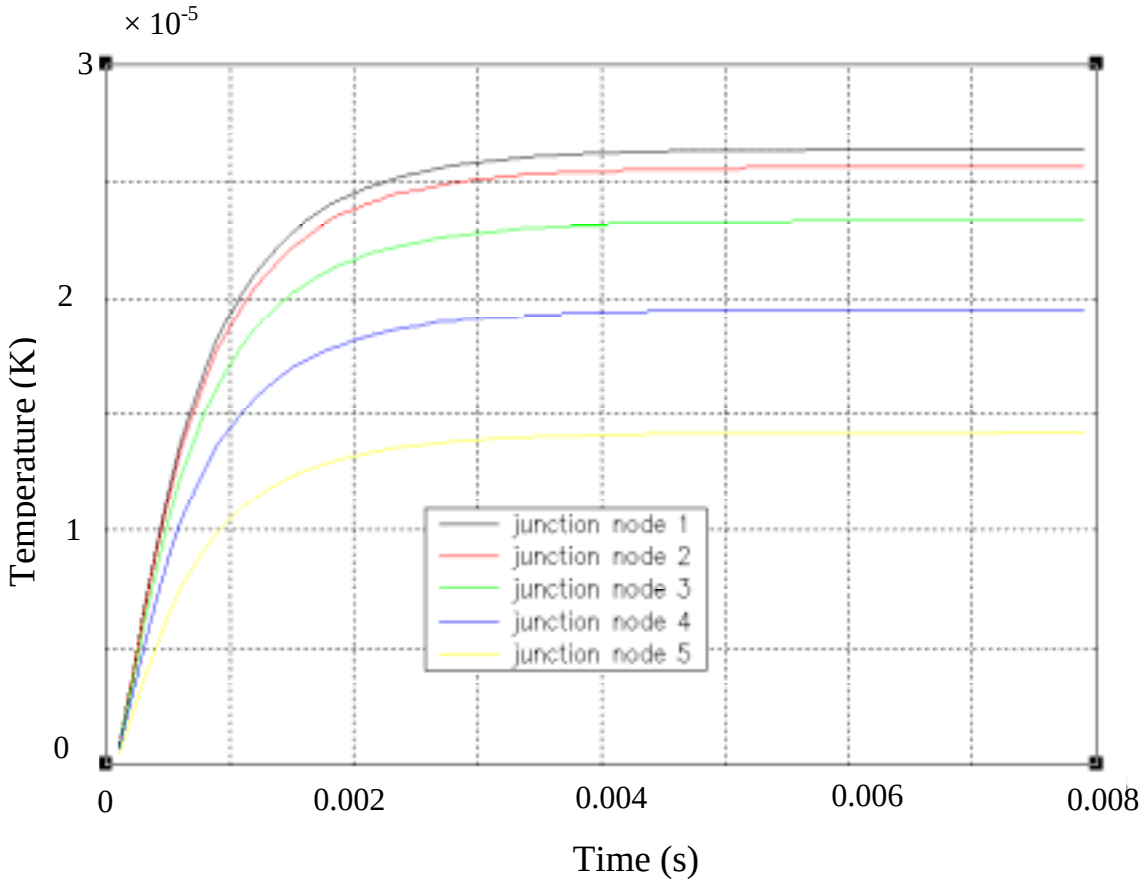

Figure 4.10. Time response of different junction nodes (active junction length of 60 μm)

Six different nodes were selected at the active junction of the thermocouple with the second configuration (i.e with an active junction length of 93 μm). They have been selected with a 22-μm space between the first five nodes and a 5-μm space between the last two nodes. These node locations may be seen in Figure 4.11, and the time response based on the different nodes is depicted in Figure 4.12.

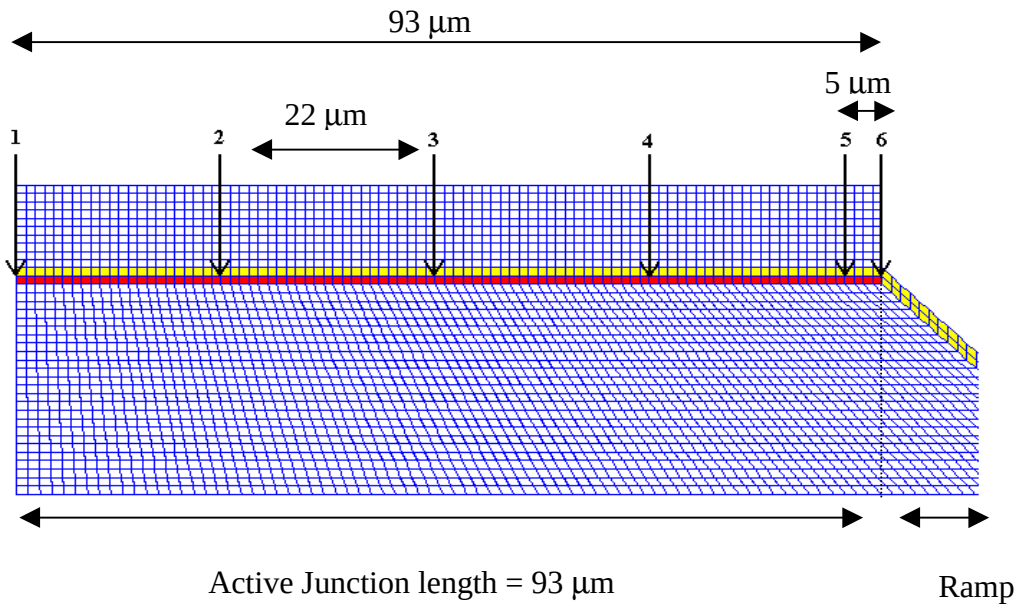

Figure 4.11. Junction nodes selected (active junction length of 93 μm)

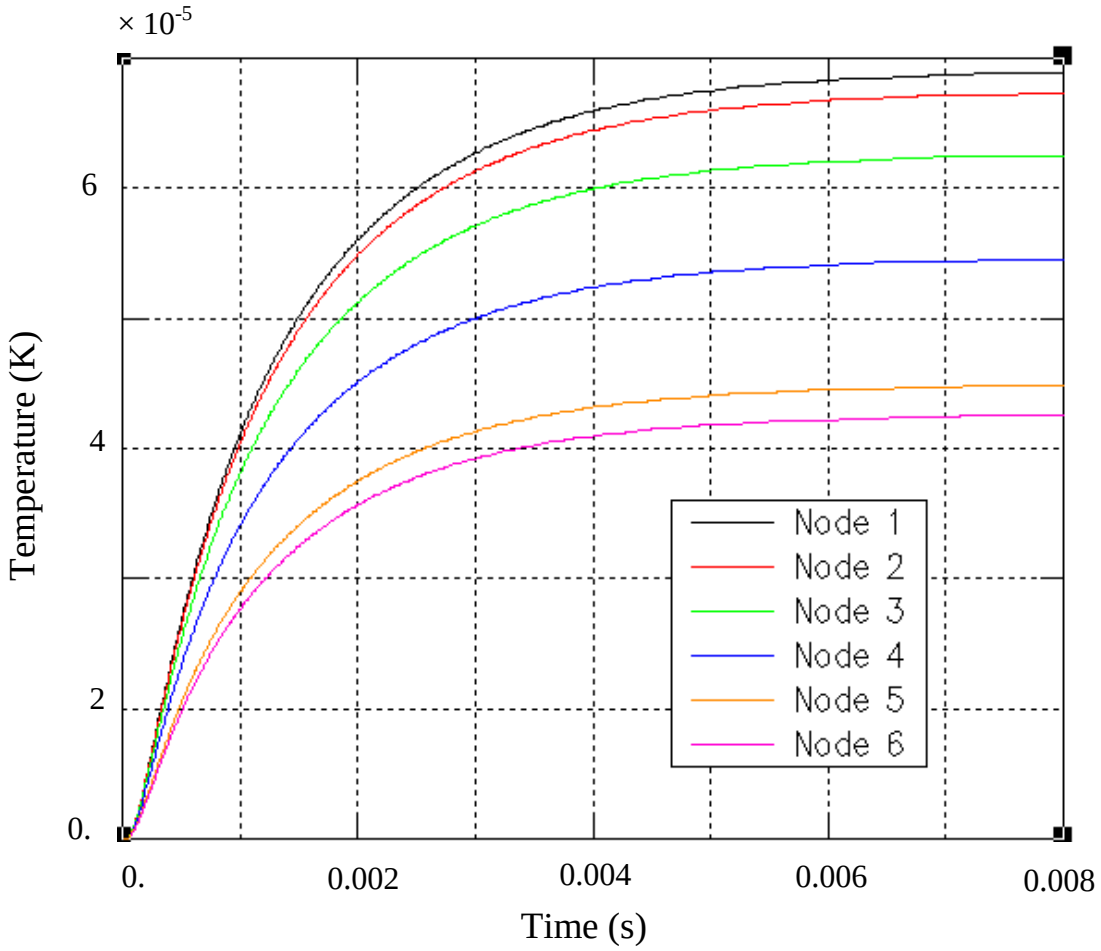

Figure 4.12. Time response of different junction nodes (active junction length of 93 μm)

Table 4.3 presents in tabular form the time constant results and the calculated rms value (using Equation 4.6) associated with all of the selected nodes as well as for the scheme where the junction nodes are averaged together.

Table 4.3. Influence of the device geometry on time constant and rms error.

	First configuration (60 μm)	Second configuration (93 μm)
Node 1	τ = 0.80 ms rms = 4.88 10^{-7}K	τ = 1.4 ms rms = 6.87 10^{-7} K
Node 2	τ = 0.79 ms rms = 4.73 10^{-7} K	τ = 1.3 ms rms = 6.56 10^{-7} K
Node 3	τ = 0.79 ms rms = 4.22 10^{-7} K	τ = 1.3 ms rms = 5.75 10^{-7} K
Node 4	τ = 0.78 ms rms = 3.50 10^{-7} K	τ = 1.3 ms rms = 4.61 10^{-7} K
Node 5	τ = 0.78 ms rms = 2.55 10^{-7} K	τ = 1.3 ms rms = 3.38 10^{-7} K
Node 6	-	τ = 1.3 ms rms = 4.89 10^{-7} K
Average across the junction	τ = 0.79 ms rms = 3.64 10^{-7} K	τ = 1.3 ms rms = 4.88 10^{-7} K

Two important results may be inferred from these data. First, the calculated time constant remains constant along the junction independent of the effective junction location used. Due to the negligible differences (at most 1.25 percent) in the schemes where the average junction nodes are used and where the highest temperature node is used, it was decided to use the transient response based on the highest temperature for the remaining analysis. The second result is that the rms error is small enough to validate the least-squares fit and thus the use of the first-order model for time response. That is, we can indeed refer to the "time constant" of this particular distributed thermal system. It should be noted that the rms error decreases as the distance between the nodes and the ramp decreases. This behavior cannot be easily explained. Figure 4.13 displays a comparison between the finite-element time response function and the "best-fit" curve from the first-order model. The term "best-fit" here refers to a curve based on using Equation 4.2 with a value of τ derived from application of Equation 4.5. The error between the two response curves (the linear interpolation of the data points and the "best-fit" curve) is plotted in Figure 4.14 and is less than 2.88 percent at any given time.

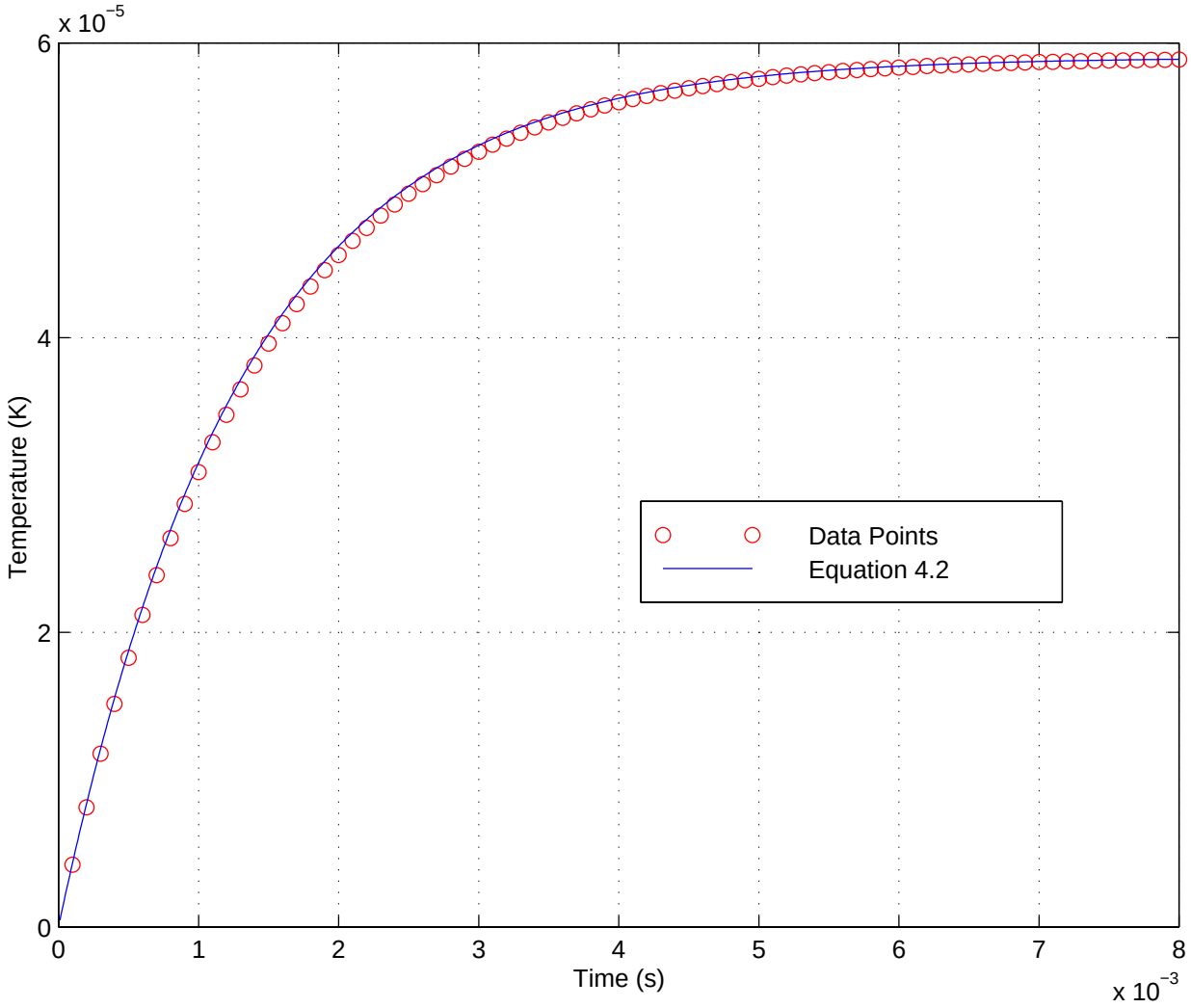

Figure 4.13. Comparison between the finite element time response function (Data points) and the "best-fit" curve (Equation 4.2) from the first-order model.

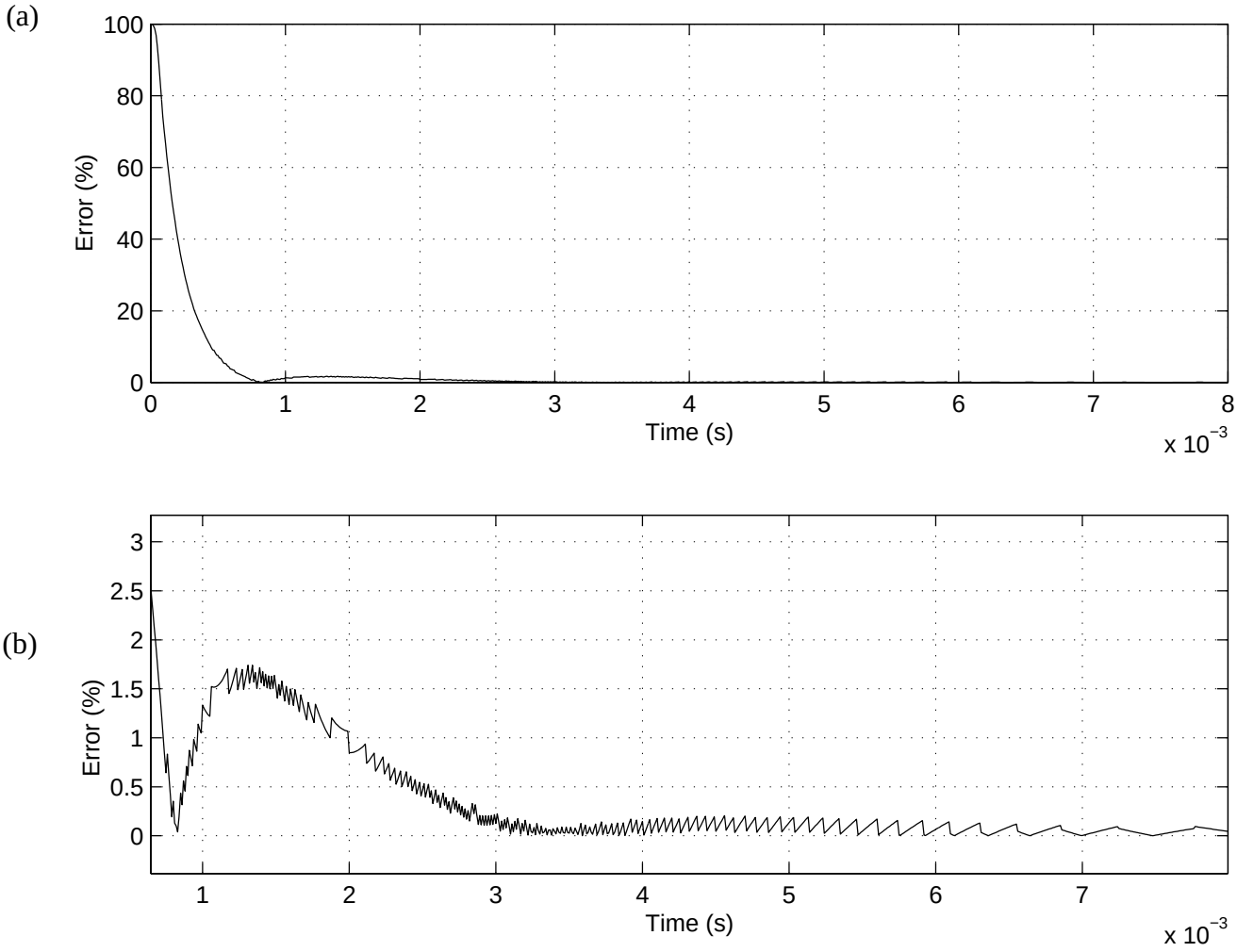

Figure 4.14. (a) Error (percent) between the finite element time response function and the "best-fit" curve (Equation 4.2), and (b) view with greater vertical resolution for $t \geq 0.7\times10^{-3}$s.

4.1.4 Conclusion

A summary comparison of both the one-dimensional and the two-dimensional model is displayed in Table 4.4.

Table 4.4. Comparison between the one-dimensional and two-dimensional models

	One-dimensional model	**Two-dimensional model** (active junction length = 93 μm)
Assumptions	One-dimensional heat flux Ramp effect neglected Reference junction not modeled	Two-dimensional heat flux Ramp effect taken into account Reference junction kept at 0 K
Sensitivity ($\mu V/W.m^{-2}$) based upon the highest temperature	0.278	0.0543
Time constant (ms)	7.8	1.4
Rms (Equation 4.6)(K)	6.89×10^{-7}	6.87×10^{-7}

The two-dimensional model yields a decrease in sensitivity and a faster time response compared to the one-dimensional model. The fact that the heat sink is twice as big in the two-dimensional case as in the one-dimensional case explains why the steady-state temperature reached is smaller in the two-dimensional case, and therefore so is the sensitivity. The fact that we obtain a time constant almost three times larger in the one-dimensional model than in the two-dimensional model with an active junction of 93 μm can be readily explained. The effect of having an aspect ratio between the heat source and the heat sink of less than one-half is that the lower steady-state temperature is going to be reached faster than in the one-dimensional model. We tentatively conclude from this study that there exists an inverse relationship between sensitivity and time response for the current thermopile design. As far as the effect of the addition of the ramp on the

sensitivity and the time response is concerned, nothing can be inferred thus far.

From the foregoing explanation one can assume that the two main geometric parameters responsible for the two-dimensional effect are the aspect ratio between the heat source and the heat sink and (likely) the slope, or length, of the ramp connecting the active junction with the reference junction. The effect of these two parameters on the sensitivity and the time response of the thermocouple is presented in the next section.

4.2 Parametric study

The results of a parametric study, including geometric parameters and boundary condition parameters, are presented in this section along with an optimized design of the thermocouple pair. The heat source (active junction) size and the slope of the ramp connecting the active and reference junctions are the two geometric parameters varied. The spatial distribution of the heat flux boundary condition was also used as a parameter in the design optimization.

4.2.1 Heat-source (active junction) size effect

Different versions of the thermocouple thermal models have been created by changing the size of the active junction while holding all other parameters constant. The active junction length was varied between 93 μm and 1000 μm in order to characterize the effect of this parameter on the sensitivity and time constant of the thermocouple. By increasing the size of the active junction, the area illuminated by heat radiation is increased. The tendency should be that the modeled performance converges to the one-dimensional results since the contribution of the ramp and the reference junction would become small compared to those of the active junction. The motivation for this study is to know how large the active junction must be relative to the rest of the design such that the two-dimensional effects described above are negligible. In other words we would like to obtain relations giving the sensitivity and time response of the thermocouple as a function of the active junction length. To determine these relationships five model versions with active junction lengths of 60, 93, 200, 500 and 1000 μm have been created. The transient response of each model

version is displayed in Figure 4.15. This figure clearly demonstrates that as we increase the active junction length the thermal time response converges to that of the one-dimensional model.

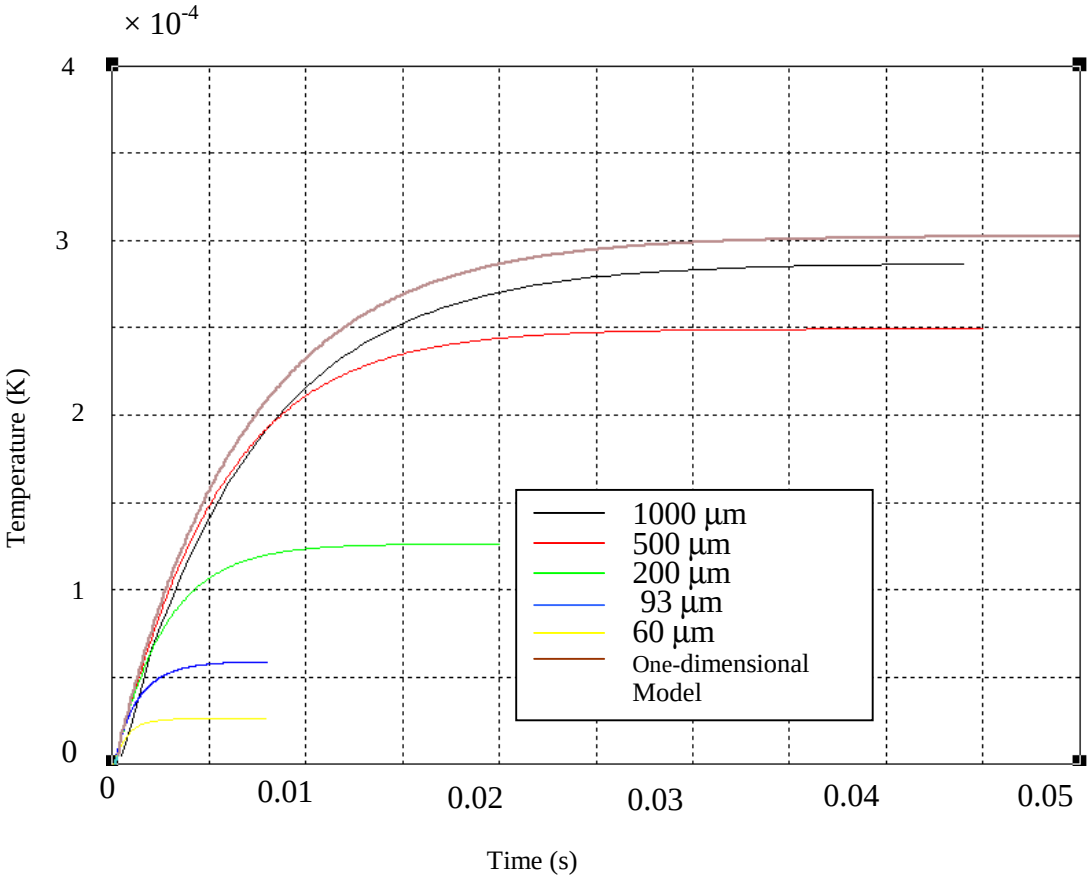

Figure 4.15. Influence of the size of the active junction on the thermal time response of the thermocouple.

Prototype detectors with active junctions over 1000 µm have been fabricated and tested by Vatell and their behavior compared to the one-dimensional model. The sensitivity of the prototypes manufactured to date vary from 0.203 to 0.276 $\mu V/Wm^{-2}$ which is in good agreement with the one-dimensional model predictions (> 0.264 $\mu V/Wm^{-2}$).

Figures 4.16 and 4.17 display the sensitivity and the time constant as a function of the active junction length. The last data points plotted for an active junction length of 5000 μm represents the one-dimensional model. This value, supposedly for an infinite active junction length, is used to fit an exponential curve of the form

$$\text{Sensitivity}(l) = 0.278\ (1 - e^{-l/350}) \qquad (4.7)$$

to the calculated points in Figure 4.16.

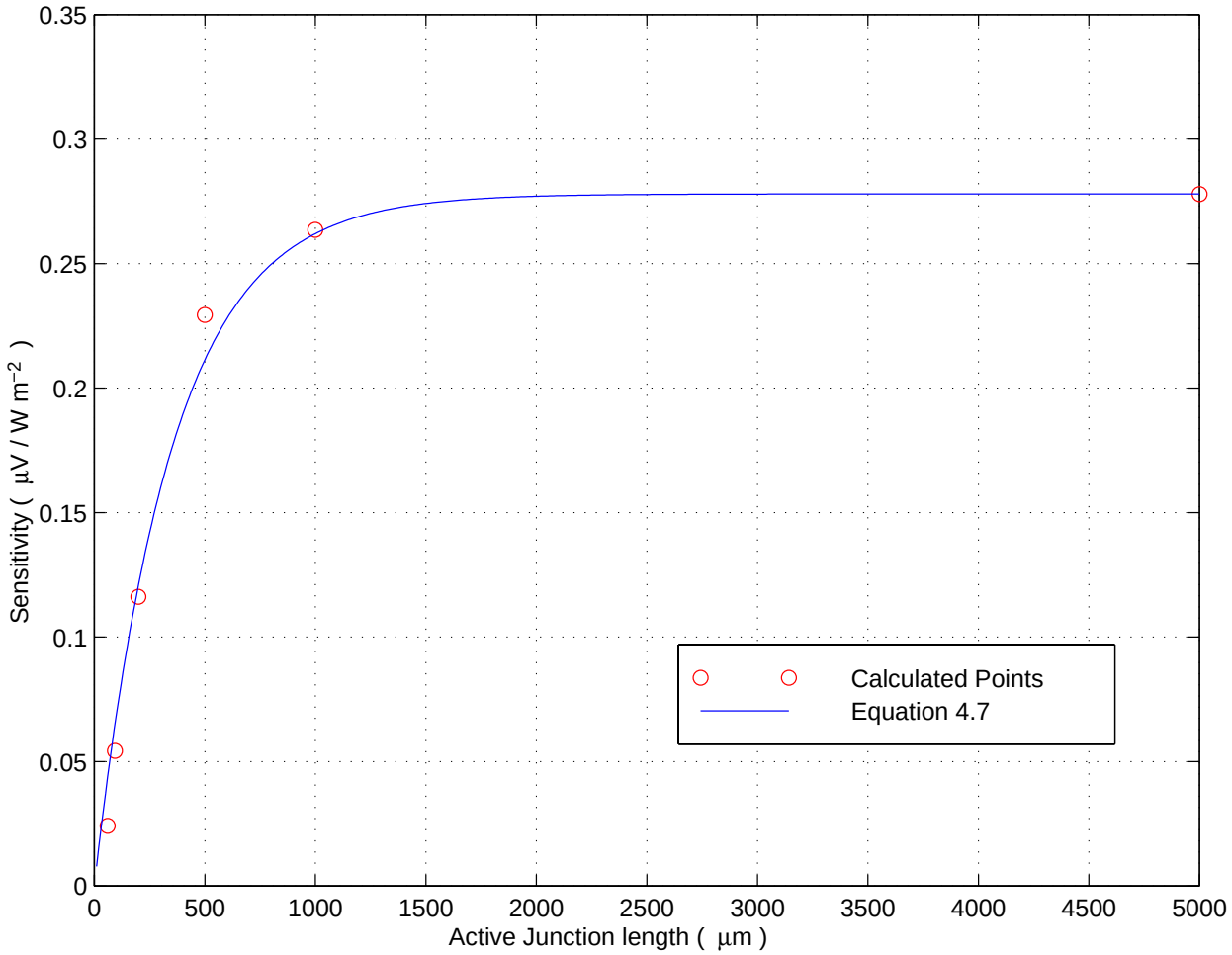

Figure 4.16. Sensitivity of the thermocouple as a function of the active junction length.

An exponential curve of the form

$$\tau(l) = 7.8\,10^{-3}\,(1 - e^{-l/420}) \qquad (4.8)$$

has been fitted to the calculated points in Figure 4.17. Here also the value of the one-dimensional time constant has been used for an infinite active junction length.

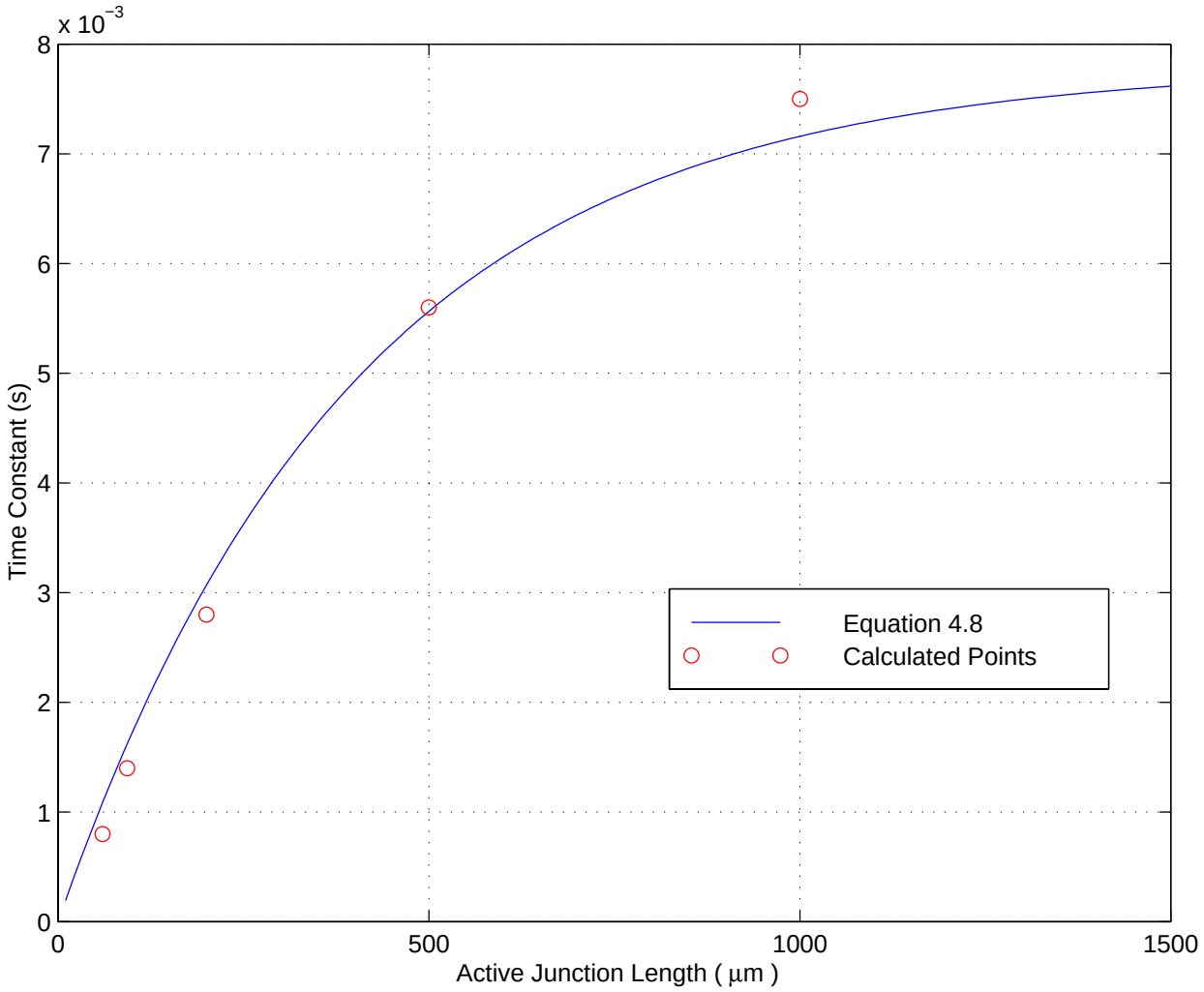

Figure 4.17. Time constant of the thermocouple as a function of the active junction length

The values of the different time constants obtained for the six cases and the associated rms error are presented in Table 4.5.

Table 4.5. Sensitivity, time constant and rms error associated for different active junction lengths

	Sensitivity ($\mu V/Wm^{-2}$)	Time Constant (ms)	Rms error Equation 4.6 (K)
1000 μm case	0.2636	6.3	8.7×10^{-6}
500 μm case	0.2294	5.5	1.63×10^{-6}
200 μm case	0.1162	2.8	1.1×10^{-6}
93 μm case	0.05430	1.4	6.87×10^{-6}
60 μm case	0.02423	0.80	4.88×10^{-7}
One-dimensional model	0.2780	6.8	6.88×10^{-7}

4.2.2 Ramp slope effect

In this section the effect on the sensitivity and time constant of the slope of the ramp connecting the active and the reference junctions is studied. It is desirable to determine an optimized ramp angle, α, so as to optimize the trade-off between the sensitivity and the time constant of the thermocouple. Five different case studies have been performed. These studies cover ramp angles, α, of 26.5, 35, 45, 50 and 63.4 deg. The two extreme design cases (α = 26.5 and α = 63 deg) and the base-line design case where α = 45 deg are illustrated in Figure 4.18.

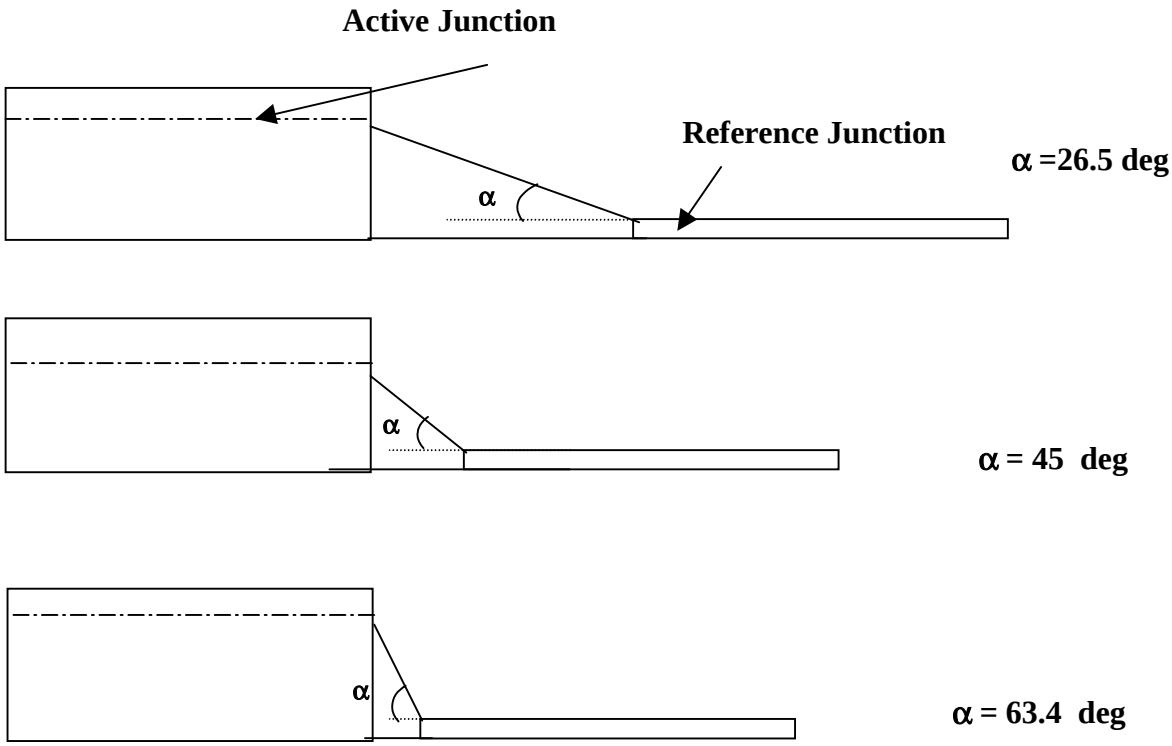

Figure 4.18. Comparison of three different designs considered in the parametric study

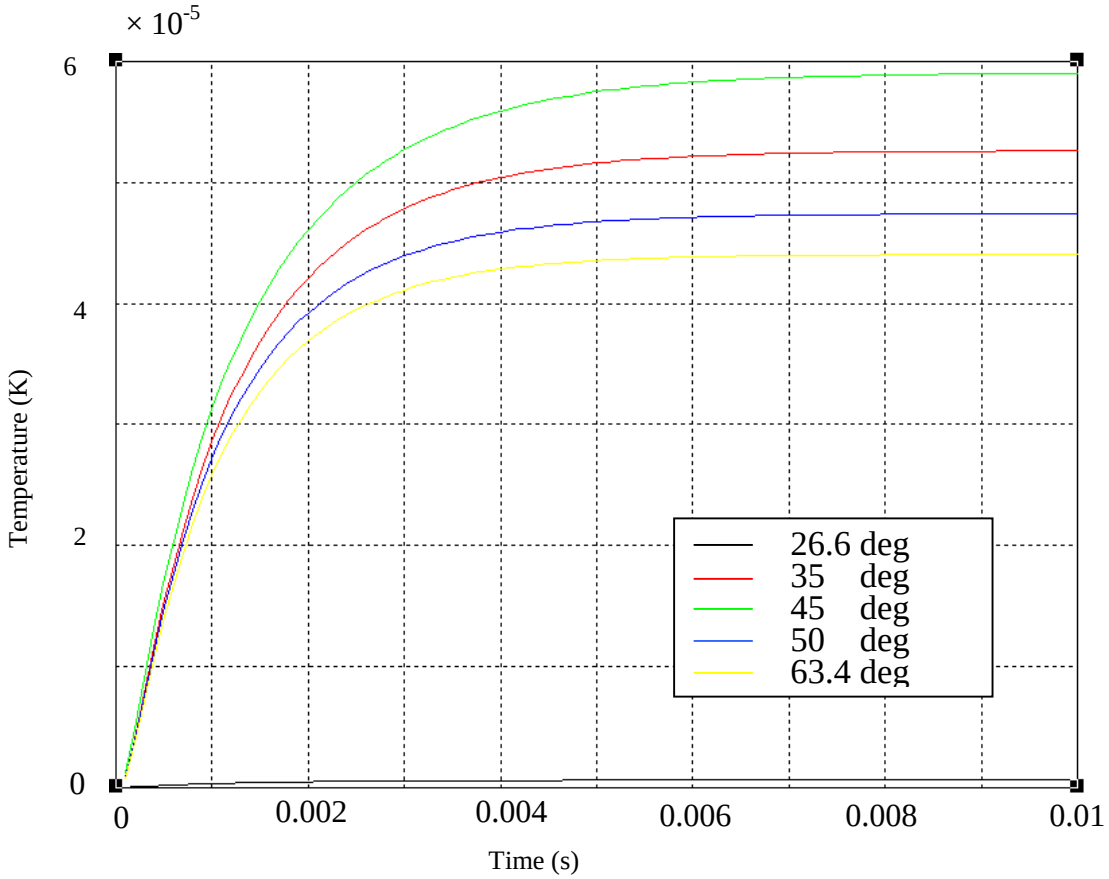

Figure 4.19. Effect of the ramp slope on the thermal time response of the thermocouple.

Figure 4.19 clearly shows that the slope of the ramp contributes to the two-dimensional effect if all other geometric parameters are held constant. However this contribution is not linear. The sensitivity increases as the angle increases from 26.5 to 45 deg and then it decreases as the angle increases beyond 45 deg up to 63 deg.

This behavior is explained by the fact that as the angle varies two other variables are inevitably varied, each of which has an opposite effect on sensitivity. The two variables are the thermal resistance of the ramp, R_t, and the aspect ratio r (the same defined in Section 4.1.2) between the heat source and the heat sink. As the ramp angle α increases the resistance R_t decreases whereas the aspect ratio r increases. When the angle α increases, the effective length l (m) decreases (Figure 4.18) and the effective cross-sectional area A_c (m^2) increases, so that according to

$$R_t = \frac{l}{k A_c}, \tag{4.9}$$

R_t decreases.

Decreasing the thermal resistance of the ramp decreases the sensitivity whereas increasing r increases the sensitivity. From the ramp angles between 26.5 to 45 deg the "resistance effect" is dominant and the sensitivity increases, and from 45 to 63 deg the "aspect ratio effect" is dominant and the sensitivity decreases.

Figure 4.20 displays the sensitivity as a function of the ramp angle α. The time constant as a function of the ramp angle α is not shown because it is essentially constant.

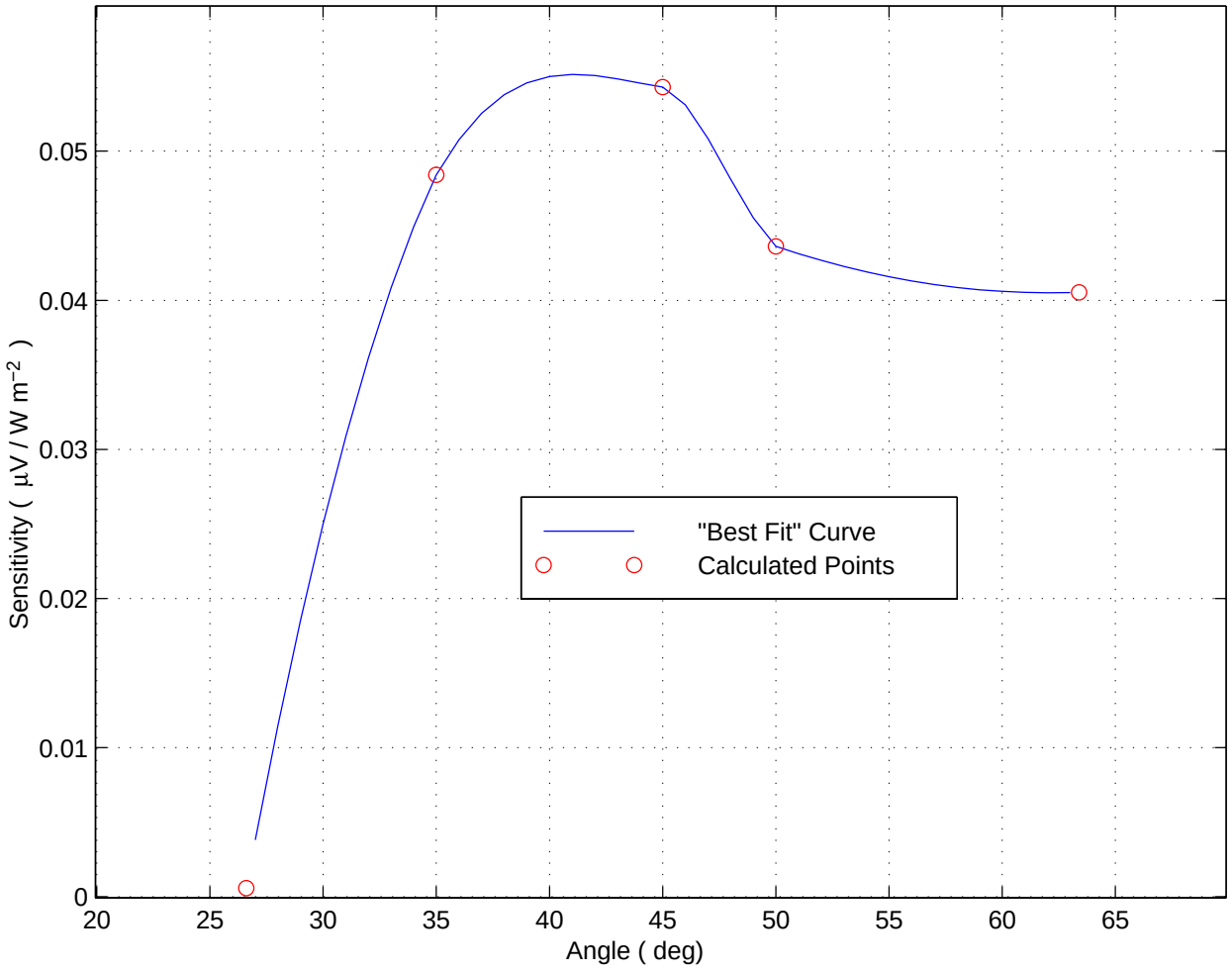

Figure 4.20. Sensitivity in function of the ramp angle α. (The "best-fit" curve is provided to help the eye follow the trend, it has no theoretical basis

The values of the sensitivity, time constant and associated rms error are presented in Table 4.6.

Table 4.6. Sensitivity, time constant and rms error for different ramp angles

α (deg)	Sensitivity ($\mu V/Wm^{-2}$)	Time Constant (ms)	Rms error (K)
26.5	582.3×10^{-6}	1.3	5.17×10^{-9}
35	0.04841	1.3	7.04×10^{-7}
45	0.05430	1.4	6.87×10^{-7}
50	0.04362	1.2	6.80×10^{-7}
63.4	0.04053	1.2	6.70×10^{-7}
One-dimensional model	0.2780	6.8	6.88×10^{-7}

4.2.3 Heat flux boundary condition

Nominally, incident radiation falls only on the active junction. In seeking to optimize the responsivity of the device a study was conducted where the heat flux boundary condition is extended to the ramp connecting the active junction and the reference junction, as shown in Figure 4.21.

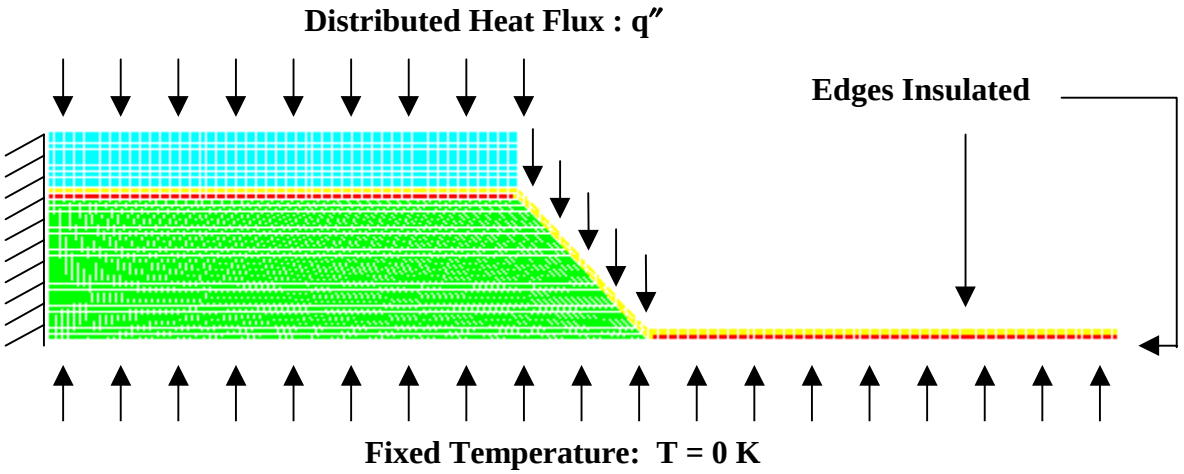

Figure 4.21. New model boundary conditions

By extending the boundary conditions to include the ramp the calculated sensitivity increased by 7 percent, from 0.0543 to 0.0584 $\mu V/Wm^{-2}$. Implementing this new boundary condition with the physical device would require slight changes in the position of the thermopile array in the cavity. The array would have to be positioned such that the incoming radiation illuminates both the active junction and the ramp connecting it to the reference junction.

The results obtained from the parametric studies presented in this chapter will be helpful in the design optimization of the thermopile linear array and provide useful feedback for the thermopile manufacturer. Tradeoffs between sensitivity and time constant must be made since decreasing the size of the thermocouple will provide faster time response but smaller sensitivities.

In the following section the possibility of having eddy currents flowing in the active junction is studied. So far it has been assumed that no current flows in the active junction even though a temperature gradient was found there. By taking into account the temperature gradient, the presence of local eddy currents is at least possible, which implies that the Peltier, Thomson and Joule effects

may have to be accounted for in the energy equation. At this point this is only a working hypothesis; experiments need to be carried out to verify it. In this section more questions are raised than answered.

4.3 Electrical model of the active junction

According to the temperature distribution results obtained in the previous sections, temperature gradients exist in the active junction. Temperature gradients may cause eddy currents to flow in the junction. Those currents are not taken into account in the current thermal model. If those currents exist the Peltier, Thomson and Joule effects must somehow be taken into account in the energy equation. An electrical model of the active junction has been formulated in order to estimate the magnitude of the currents. The active junction of the 60-μm active junction model has been discretized into cells with the temperature fixed at different values at the two ends. The cells created correspond to the finite element control volumes used in the thermal model. Figure 4.22 displays 60 discrete cells of 1-μm length each (61 nodes) and the associated electrical model. The temperature gradient ΔT_i between Node i and Node i+1 creates a current I_i in cell i. The generated voltages V_i (V) can be calculated using the Seebeck effect Equation 4.2, relating the emf V_i to the temperature gradient ΔT_i (K) and the Seebeck coefficient $S_{ZnSb-Pt}$ (μV/K).

$$V_i = S_{ZnSb-Pt}\,\Delta T_i \ . \tag{4.10}$$

The resistance R_1 (Ω) represents the zinc-antimonide resistance and R_2 (Ω) the platinum resistance. The resistances R_1 and R_2 are calculated based on the resistivity ρ_1 and ρ_2 (Ωm) of the associated material according to the relationship

$$R = \frac{\rho L}{A} \quad , \tag{4.11}$$

where L (m) is the length of material conducting the current flow and A (m^2) is the cross-sectional area.

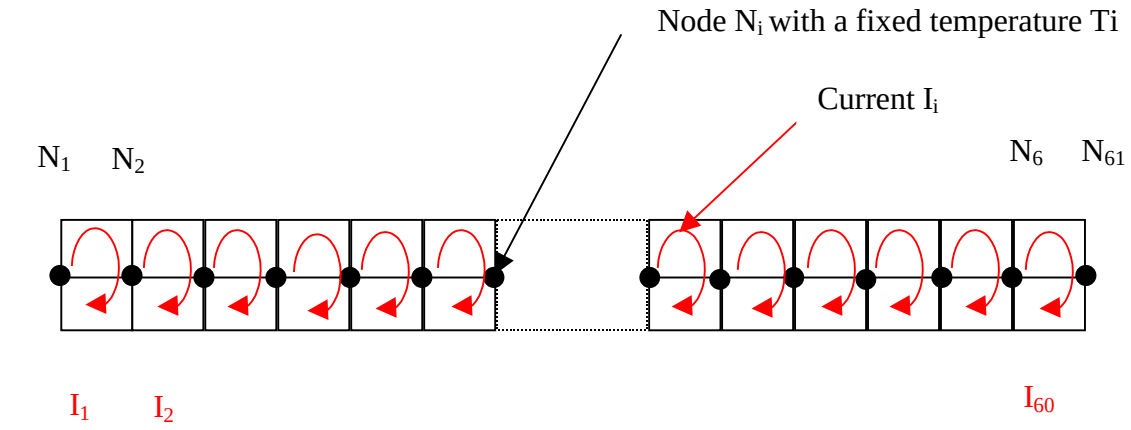

(a)

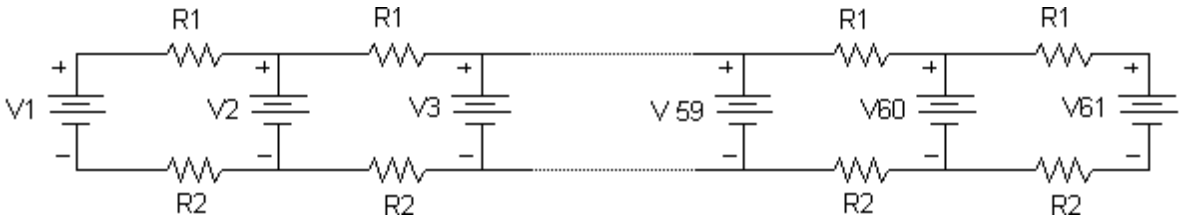

(b)

Figure 4.22. The distributed junction represented as (a) sixty discreet cells (61 nodes) and (b) the associated electrical model.

In order to evaluate the different currents I_i flowing in the 60 cells, the algebraic system

$$\begin{aligned} &V_1 + R_1 I_1 - V_2 + R_2 I_1 = 0 \\ &V_2 + R_1 I_2 - V_2 + R_2 I_2 = 0 \\ &\vdots \\ &V_{60} + R_1 I_{60} - V_2 + R_2 I_{60} = 0 \end{aligned} \tag{4.12}$$

was solved for each I_i. This leads to the equivalent system

$$I_k = \frac{(V_{k+1} - V_k)}{R_1 + R_2} \quad , \; k = 1, 2, \ldots, 60 \quad . \tag{4.13}$$

Using Equations 4.2 and 4.3 we obtain

$$I_k = \frac{(T_{k+1} - T_k)\; S_{ZnSb-Pt}\; A}{(\rho_1 + \rho_2)\, L} \quad , k = 1,2,\ldots,60 \quad , \tag{4.14}$$

where T_k is the temperature (K) at node k calculated by the finite element model.

The idea is to modify the energy equation, Equation 3.3, by adding a heat source term q'''_k (W) of the form

$$q'''_k = R\, I_k^{\,2} + P_{AB}\; I_k + \sigma_{AB} \frac{\Delta T}{\Delta x} I_k \tag{4.15}$$

for each node k of the finite grid through which an current I_k flows. Equation 4.6 takes into account the power due to the Peltier, Thomson and Joule effects. The new temperature distribution could be calculated by the finite difference method. The unresolved problem is to determine the coefficients associated with the Peltier and Thomson effect. To accomplish this additional experiments would need to be carried out. For example, we could take a rod of zinc-antimonide with a temperature gradient. We could force a current through it and then be able to measure the heat loss (if the current goes with the temperature gradient). The Thomson coefficient of the rod of zinc-antimonide could be calculated, knowing how much energy has been dissipated by the Joule effect.

A temperature gradient of 1.213×10^{-5} K is found at the two ends of a 60-μm active junction. The eddy current flowing in the active junction due to this temperature gradient would be on the

order of 0.2 mA and the heat released by the Joule effect would then be on the order of 4.24×10^{-15} W, which is surely negligible. It might be expected that the heat absorbed and released by the Peltier and Thomson effects would also be of the same order of magnitude, and therefore also negligible.